A GENERALIZED APPROACH FOR ATOMIC FORCE MICROSCOPY IMAGE RESTORATION WITH BREGMAN DISTANCES AS TIKHONOV REGULARIZATION TERMS

Geraldo A. G. Cidade[1], Celia Anteneodo[1], Nilson C. Roberty[2] and Antônio J. Silva Neto[3,2]*
[1]Instituto de Biofísica Carlos Chagas Filho - CCS - Universidade Federal
do Rio de Janeiro, CEP 21949-900, Rio de Janeiro, RJ, Brazil,
gcidade@biof.ufrj.br and celia@cbpf.br
[2]Nuclear Engineering Program - COPPE - Universidade Federal do Rio de Janeiro,
CP 68509, CEP 21945-970, Rio de Janeiro, RJ, Brazil,
nilson@lmn.con.ufrj.br and ajsneto@lmn.con.ufrj.br
[3]Instituto Politécnico, Universidade do Estado do Rio de Janeiro, CP 97282,
CEP 28601-970, Nova Friburgo, RJ, Brazil, ajsneto@iprj.uerj.br

ABSTRACT

Tikhonov's regularization approach applied to image restoration, stated in terms of *ill-posed* problems, has proved to be a powerful tool to solve noisy and incomplete data. This work proposes a variable norm discrepancy function as the regularization term of a Tikhonov expression, where the cross-entropy functional was derived. Our method was applied to true Atomic Force Microscopy (AFM) images obtained from biological samples, producing satisfactory results towards the most probable sample morphological aspect. These images represent a mapping of local interaction forces exerted between a reduced scaled AFM sensing tip and the biological sample surface, kept alive in aqueous or air enviroment.

Keywords: Image restoration, regularization, atomic force microscopy, biological sample.

---

* Corresponding author. A preliminary version of this paper has been presented at the 3rd International Conference on Inverse Problems in Engineering: Theory and Practice [1].

INTRODUCTION

The Atomic Force Microscopy (AFM) technique [2] consists, basically, on the production of force images, formated like tridimensional photographs, by means of very small sensing tips, used to map the interaction between the sample and the tip. The greatest advantage of the AFM technique is its ability to image the surface of randomly distributed macromolecules *in situ*, if not *in vivo*, which opens a new promising approach in the structural biology field [3], complementing well with other techniques such as electron-microscopy and X-ray diffraction. Among several powerful capabilities, the AFM technique, when applied to biological samples, allows the visualization of microscopic structure features from cell membrane surfaces, like proteins, in the nanometer range [4,5]. For images in this range scale, the interaction between the tip an the sample can produce blurred images, with the blurring being related to the tip geometry (operator). Besides the blurring effect, additive noise is also present. Being an *ill-posed* problem, a direct inversion is not directly applied to deconvolve the blurred image.

The solution of *ill-posed* problems, by means of regularization [6], resulted in a substantial number of developments in different application fields, such as astronomy [7] and scanning-tunneling microscopy [8]. For the solution of any direct problem, three essential requirements have to be satisfied: *existence*, *uniqueness* and *stability*. Depending strictly on the quality of the operator in presence of noise, at least one of these qualifiers may not be met on the formulation of inverse problems. The regularization theory applied to image restoration is based on the trade-off between fidelity to the data and smoothness of the solution in the space domain, converting an *ill-posed* problem into a *well-posed* one [9], deriving an acceptable approximation towards the most feasible solution (original image).

MATHEMATICAL FORMULATION OF THE DIRECT AND INVERSE PROBLEMS

When the operator intrinsically exhibits geometrical limitations, as is the case of the cantilever's tip used in AFM to produce sample scanning images in the nanometer range, considerable blurring effects (tip-to-sample convolutions) may occur. Also due to the extremely small scale, other undesirable additive perturbations (noise) could lead to images with poor signal-to-noise ratios. Differently from image enhancement [10], the main goal in image restoration is to make the processed image to be as close to the true image as possible in regard to intensity distribution. Therefore, the effects of blurring and additive noise may be outlined as:

$$y = Bx + n, \tag{1}$$

where $y \in \psi$ represents the real image, $x \in \Im$ the original image (being $\Im$ and ψ Hilbert spaces), B a compact operator, described by a point-spread function (PSF) matrix of the imaging system ($B : \Im \to \psi$) and n the additive noise, generally of Gaussian type. Considering only the first term in the right hand side of Eq. (1), the image (without additive noise) is described by a Fredholm equation of the first kind [11]:

$$y(z) = \int b(z,w)\varphi(w)dw \tag{2}$$

where $\varphi(w)$ represents the expected unique solution obtained along the restoration process, located near the primitive intensities in the domain region, in analogy to x in Eq. (1).

This problem is considered *well-posed* if, for each $y \in \psi$, a unique solution $x \in \Im$ does exist, depending continuously on the observed data, otherwise it would be *ill-posed* [12], with no apparent solution if the B operator is a square matrix, with det(B)=0. Based on this argument, the inverse problem

$$x = B^{-1}y \tag{3}$$

was considered *ill-posed* [13]. As the eigenvalues accumulate in zero [6], a small perturbation in the data y yields a large perturbation in the solution x [9]. Therefore, the inverse problem is solved as a finite dimensional optimization problem in which we minimize a functional such as the one with the square residues

$$L(x) = \|y - Bx\|^2 \tag{4}$$

This is the well known least squares method [11].

TIKHONOV'S REGULARIZATION

The functional to be minimized may also be constructed based on the Bayesian argument of conditioned probability [8]. Searching for an adequate compromise between accuracy and stability, a Tikhonov regularizing term is added to the norm given by Eq. (4)

$$Q(\hat{x}) = \frac{1}{2} \| y(i,j) - \sum_{k=-N}^{N} \sum_{l=-N}^{N} b(k,l).\hat{x}(i+k, j+l) \|^2 + \alpha S \quad (\alpha > 0; i = j = 1,2,...,M) \tag{5}$$

generating a regularized solution to this problem [14], based on the classical Tikhonov regularizing functional [11], where *y(i,j)* represents the acquired image, *b(k,l)* the PSF, $\hat{x}$ the estimated data that we want to determine, and αS the regularization term, where parameter α determines the trade-off between the accuracy and the stability of the solution; *(i,j)* is a specific pixel of the total M x M image pixels, and the blurring discrete operator *b(k,l)* convolves *(2N+1) x (2N+1)* pixels around that specific one. Depending on the image characteristics, the functional S can be defined by any prior function that imposes no correlation on the image for which there is no evidence in the available data (maximally noncommittal).

Although other general functionals can be used [15], like the Csiszer's measure [16], this work proposes a general functional, which we call *q-discrepancy* (also related to Tsallis entropy [17,18], basis of a new thermostatistical formalism) to derive a family of regularizing terms using Bregman distances of convex projections [19,20].

We first define a *q-discrepancy* functional [20]

$$\eta_q(x) = \frac{1}{1+q} \sum_{p=1}^{M \times M} \{ x_p \frac{x_p^q - m^q}{q} \} \tag{6}$$

that gives the deviation of an expected value x, enhanced by the q power, from a prior information given by a measure m of the space of unknowns.

As our main objective is to construct a family of regularization terms S for Tikhonov's functional given in Eq.(5), we use Bregman's distances [19] with the convex functions given by the *q-discrepancy* shown in Eq.(6),

$$S = D_q(\hat{x}, \bar{x}) = D(\eta_q(\hat{x}), \eta_q(\bar{x})) \tag{7}$$

where the Bregman distance comprehends the second or higher order terms of a Taylor's expansion,

$$D(\eta_q(\hat{x}), \eta_q(\bar{x})) = \eta_q(\hat{x}) - \eta_q(\bar{x}) - \left\langle \nabla \eta_q(\bar{x}), \hat{x} - \bar{x} \right\rangle \tag{8}$$

and $\hat{x}$ represents the estimated image data values and $\bar{x}$ describes a prior reference model, stated, for example, in terms of the weighted average from the acquired image data, representing an equally likely distribution.

It is straightforward to calculate the gradient from Eq.(6),

$$\left[\nabla \eta_q(x)\right]_p = \frac{1}{1+q}\left\{\frac{x_p^q - m^q}{q} + x_p^q\right\} \tag{9}$$

Introducing Eqs. (6) and (9) into Eq.(8), one obtains

$$S = D_q(\hat{x}, \bar{x}) = \frac{1}{1+q}\sum_{p=1}^{M\times M}\left\{\ \hat{x}_p\left[\frac{(\hat{x}_p)^q - (\bar{x}_p)^q}{q}\right] - (\bar{x}_p)^q(\hat{x}_p - \bar{x}_p)\ \right\} \tag{10}$$

Therefore, the main contribution of this paper is to propose a general regularization term constructed with Bregman distances, based on on the *q-discrepancy* functional, for the restoration of AFM biological images. This general regularization functional is capable to derive, as particular cases, both the energy and the entropy regularization terms, depending on the value of q; for q=1, from Eq. (10), we obtain,

$$S = D_q(\hat{x}, \bar{x}) = \frac{1}{2}\sum_{p=1}^{M\times M}\left\{\ \hat{x}_p(\hat{x}_p - \bar{x}_p) - \bar{x}_p(\hat{x}_p - \bar{x}_p)\ \right\} = \frac{1}{2}\sum_{p=1}^{M\times M}\ (\hat{x}_p - \bar{x}_p)^2 \tag{11}$$

known as the energy functional.

Using the expansions

$$(\hat{x}_p)^q = e^{q\ln \hat{x}_p} = 1 + q\ln\hat{x}_p + \frac{q^2}{2}(\ln\hat{x}_p)^2 + \ldots \tag{12a}$$

$$(\bar{x}_p)^q = e^{q\ln \bar{x}_p} = 1 + q\ln\bar{x}_p + \frac{q^2}{2}(\ln\bar{x}_p)^2 + \ldots \tag{12b}$$

the term within brackets in Eq. (10) is written as

$$\left[\frac{(\hat{x}_p)^q - (\bar{x}_p)^q}{q}\right] = \ln\frac{\hat{x}_p}{\bar{x}_p} + \frac{q}{2}\left\{(\ln\hat{x}_p)^2 - (\ln\bar{x}_p)^2\right\} + \ldots \tag{13}$$

Substituting Eq. (13) into Eq. (10) and taking the limit when $q \to 0$, one obtains

$$S = -\sum_{p=1}^{MxM}\left[\hat{x}_p\ln\frac{\hat{x}_p}{\bar{x}_p} - (\hat{x}_p - \bar{x}_p)\right] = -\sum_{p=1}^{MxM}\left[\hat{x}_p - \bar{x}_p - \hat{x}_p\ln\frac{\hat{x}_p}{\bar{x}_p}\right] \tag{14}$$

known as the cross-entropy functional.

One can see that varying the value of the q parameter a family of regularization terms is constructed. The advantage of using the approach proposed here is that in some applications the energy functional yields better results while in other applications the use of the entropy functional may be more appropriate. The implementation of an algorithm with a more general functional, that includes as particular cases such commonly used functionals, allows a broader range of investigations in which one may even interpolate or extrapolate the entropy and energy functionals. Results obtained so far have shown that larger values of q, i.e. $q>1$, gives restored images with enhanced contrast, which can be of interest if one is trying to find deviations from an original image that is supposedly smooth. For smaller values of q (even negative) we have observed in our numerical simulations that smoothness has been introduced in the restored images.

In this paper the results obtained with the cross-entropy functional, i.e. $q \to 0$, will be presented. Results obtained with q values that interpolate or extrapolate the entropy and the energy functionals wil be presented elsewhere.

For computational purposes the cross-entropy functional given by Eq. (14) will be written as

$$S = -\sum_{i=1}^{M}\sum_{j=1}^{M}\left[\hat{x}(i,j) - \bar{x}(i,j) - \hat{x}(i,j)\ln\frac{\hat{x}(i,j)}{\bar{x}(i,j)}\right] \tag{15}$$

The functional Q, given by Eq. (5), will be minimized when both the squared residues, given by Eq. (4), and discrepancies tend to be minimal (maximal configurational entropy); the *maximum entropy* criterion, proposed by Jaynes [16], applied to image restoration [21], establishes that *"of all feasible (possible) solutions, there should be used the one that has the maximum configurational entropy"* [10].

In order to minimize the Q functional we write the critical point equation $\partial Q / \partial \hat{x} = 0$, yielding a system of non-linear equations [22]

$$F(\hat{x}) = 0 \tag{16}$$

i.e.,

$$F_{rs} = \frac{\partial Q}{\partial \hat{x}_{rs}} = -\sum_{i=1}^{M}\sum_{j=1}^{M}\left[y(i,j) - \sum_{k=-N}^{N}\sum_{l=-N}^{N} b(k,l)\,\hat{x}(i+k, j+l)\right] b_{r-i,s-j} + \alpha \ln\frac{\hat{x}(r,s)}{\bar{x}(r,s)} = 0, \qquad r,s = 1,2,...,M \tag{17}$$

where we have used the following results

$$\frac{\partial \hat{x}(i+k, j+l)}{\partial \hat{x}_{rs}} = \delta_{i+k,r}\,\delta_{j+l,s} \tag{18}$$

$$\sum_{k=-N}^{N}\sum_{l=-N}^{N} b_{kl}\,\frac{\partial \hat{x}(i+k, j+l)}{\partial \hat{x}_{rs}} = b_{r-i,s-j} \tag{19}$$

For a typical image of 256 x 256 pixels, i.e. M=256, there are 65536 unknowns. To solve this system of non-linear equations we use the iterative multivariable Newton-Raphson method, in which a linearization is obtained using a Taylor's expansion, retaining only terms up to the first order

$$F(\hat{x}) = F(\hat{x}\,|^{p}) + \sum_{m=1}^{M}\sum_{n=1}^{M}\left.\frac{\partial F}{\partial \hat{x}_{mn}}\right|^{p} \Delta\hat{x}_{mn}\Big|^{p} + \vartheta(\Delta x_{mn}^{2}) = 0 \tag{20}$$

where p represents the iteration counter, with new estimates for the unknowns being calculated with

$$\hat{x}\,|^{p+1} = \hat{x}\,|^{p} + \gamma.\Delta\hat{x}\,|^{p} \tag{21}$$

where γ is used as a gain factor to produce more stability along the iterative process as the convergence takes place towards the expected solution.

At every step of the iterative procedure we have to solve the linear sparse system of algebraic equations represented by Eq. (20), where

$$\frac{\partial F_{rs}}{\partial \hat{x}_{mn}} = \sum_{k=-N}^{N} \sum_{l=-N}^{N} b_{kl} b_{r-m+k,s-n+l} + \frac{\alpha}{\hat{x}_{rs}} \delta_{rm} \delta_{sn} \tag{22}$$

knowing that similarly to Eqs. (17) and (18),

$$\frac{\partial \hat{x}(i+k,\, j+l)}{\partial \hat{x}_{mn}} = \delta_{i+k,m} \delta_{j+l,n} \tag{23}$$

$$\sum_{k=-N}^{N} \sum_{l=-N}^{N} b_{kl} \frac{\partial \hat{x}(i+k,\, j+l)}{\partial \hat{x}_{mn}} = b_{m-i,n-j} \tag{24}$$

Taking advantage of the system sparsity, as well as the diagonal dominance induced by the blurring operators considered in this work, we have used the iterative Gauss-Seidel method [10,22] to obtain an approximation of the solution for this linear system.

An inner loop with iteration counter *t* is considered with new estimates for the correction term $\Delta\hat{x}$ being calculated from

$$\Delta \hat{x}_{rs}\Big|^{p,t+1} = -\frac{1}{\left.\dfrac{\partial F_{rs}}{\partial \hat{x}_{rs}}\right|_{\hat{x}|^{p,t}}} \left\{ F_{rs}\Big|_{\hat{x}|^{p,t}} + \sum_{\substack{m=1 \\ m \neq r}}^{M} \sum_{\substack{n=1 \\ n \neq s}}^{M} \left.\frac{\partial F_{rs}}{\partial \hat{x}_{mn}}\right|_{\hat{x}|^{p,t}} \Delta \hat{x}_{mn}^{p,\tilde{t}} \right\}, \quad r,s = 1,2,...,M, \qquad \Delta \hat{x}^{p,0} = 0 \tag{25}$$

where $\tilde{t}$ can be *t* or *t+1*, depending on how the sweep through the pixels is done. In a given inner loop iteration *t+1* (Gauss-Seidel), as soon as a new estimate for the corrections $\Delta \hat{x}_{rs}\Big|^{p,t+1}$ is calculated, it becomes avaiable for the use in the computation of the following $\Delta \hat{x}_{rs}$ that will be updated.

Figure 1 illustrates the algorithm's simplified flow chart, which uses the Q_{min} criterion to stop the process. The program was written in C language, using the C++ Builder Server/Client© platform from Borland Inc., providing an user friendly interface.

RESULTS AND DISCUSSION

In our case, the cantilever's tip effects (blurring) present in the 256 x 256 pixels AFM images can be clearly observed in dimensions less than or equal to 1μm x 1μm. For this reason, in this scale, postacquisition processing (image restoration) becomes necessary to reveal important specimen's structural and functional features. The mathematical representation of the tip geometry (blurring operator) was chosen to be similar to a Gaussian tridimensional distribution [8], with adjustable variance (σ^2). The cross-entropy functional, derived from the Bregman distance [19] based on the *q-discrepancy* functional ($q \to 0$) [1,18], was used in the regularization term.

Figure 2 illustrates a true 1μm x 1μm AFM biological image of an eritroblast in leukemia pathology, whose details were improved (Figure 3) after running the algorithm, assuming a 9 x 9 deconvolution Gaussian matrix (DGM) with σ^2 =10, using α=0.03 and γ=0.2.

(Figure 2)
(Figure 3)

Figure 4 shows another true 600 nm x 600 nm image of the same sample, restored with
(Figure 4)
different Gaussian tip profiles (Figs 5 and 6), using the same α and γ values as in Figure 3. Figure 5 shows minor improvements in its contrast contents for a 9 x 9 DGM with σ^2=10, whereas Figure 6 reveals more visible contours after deconvolving the true image with a 15 x 15 DGM with σ^2=40; usual contrast and brightness treatments were applied to all images.
(Figure 5)
(Figure 6)

In the test case involving Figures 4-6, besides the image reconstruction we make an attempt to identify the parameters of the blurring operator already characterized as a tridimensional Gaussian distribution [22].

We must stress that for the expert observer the structures added to the reconstructed images do not correspond to artifacts. They bring relevant contrast information that would be lost if other techniques, such as Fourier Transform (FFT), had been applied.

In order to attenuate the presence of artificial structures in the image, like the border effects induced by external data around the image frame, we restricted the action of the deconvolution matrixes' indexes along these critical regions, using only the image's indexes, which produced good results.

We should emphasize that, as expected, the results obtained depend on the choice of parameter α. Therefore, the proper choice (determination) of α is an important aspect of the inverse problem here described.

In all test cases presented in this work we have performed a systematic numerical experimentation in which we vary the value of the regularization parameter α, looking for the one that yielded the minimum value for Tikhonov's functional given by Eq. (5). In this sense we may say that we obtain a quasi-optimal restoration, in which for a given value of the q parameter ($q \to 0$, for the cross-entropy functional used in all test cases presented) we try to find, with numerical experiments, the optimal value of the regularization parameter that gives the minimum value of Q.

We have also done numerical experiments in order to determine the best value of the gain factor used in the multivariable Newton method for the solution of the linear system (outer loop in Fig. 1) to converge as fast as possible and exhibit good accuracy.

CONCLUSIONS

The results obtained so far have been very encouraging. At the moment we are finalizing the implementation of the general regularization term based on the *q-discrepancy* described previously. Our future goal is to determine which value for q yields the best solution of the reconstruction problem. The results of such investigation will be presented elsewhere.

With respect to the regularization parameter in Eq. (5), one comment is in order. The determination of an optimal parameter is possible, and has already been done for the squared residues norm [11], but is computationally involved. Therefore, the most common approach is to perform numerical experimentations for the estimation of such parameter [8]. As described previously, the results presented in this paper were obtained applying this approach.

We have also in mind to develop and implement an automatic correction of the regularization parameter along the iterative procedure, that may improve the estimates producing even better results [23].

ACKNOWLEDGMENTS

The authors thank Prof. Gilberto Weissmüller from Instituto de Biofísica Carlos Chagas Filho – UFRJ for the AFM biological images. This work was supported by FAPERJ and CNPq.

REFERENCES

1. Cidade, G.A.G., Anteneodo, C., Roberty, N.C. and Silva Neto, A.J., A Generalized Approach for Atomic Force Microscopy Image Restoration with Bregman Distances as Tikhonov Regularization Terms, Proc. 3rd International Conference on Inverse Problems in Engineering: Theory and Practice, Port Ludlow, Washington, USA, 1999.
2. Binnig, G., Quate, C.F. and Gerber, CH., Atomic Force Microscope, Phys. Rev. Lett., 56, 9, 1986, pp. 930-933.
3. Glaeser, R.M., Probing Toward Atomic Resolution in Molecular Topography, Proc. Natl. Acad. Sci.USA, 91, 1994, pp. 1981-1982.
4. Amato, I., Candid Cameras for the Nanoworld, Science, 276, 1997, pp. 1982-1985.
5. Oberleithner, H., Brinckmann, E., Schwab, A. and Krohne, G., Imaging Nuclear Pores of Aldesterone-Sensitive Kidney Cells by Atomic Force Microscopy, Proc. Natl. Acad. Sci.USA, 91, 1994, pp. 9784-9788.
6. Tikhonov, A.N. and Arsenin, V.Y., Solutions of Ill-Posed Problems, Wiley, New York, 1977.
7. Gull, S.F. and Daniell, G.J., Image Reconstruction from Incomplete and Noisy Data, Nature, 272, 20, 1978, pp. 686-690.
8. Kokaram, A.C., Persad, N., Lasenby, J., Fitzgerald, W.J., Mckinnon, A. and Welland, M., Restoration of Images from the Scanning-Tunneling Microscope, Applied Optics, 34, 23, 1995, pp. 5121-5132.
9. Kang, M.G. and Katsaggelos, A.K., General Choice of the Regularization Functional in Regularized Image Restoration, IEEE Trans. Image Process., 4, 5, 1995, pp.594-602.
10. Wu, N.,The Maximum Entropy Method, Springer Series in Information Sciences, 1997.
11. Kress, R., Applied Mathematical Sciences, 82, Springer Verlag, 1989.
12. Karayiannis, N.B. and Venetsanopoulos, A.N., Regularization Theory in Image Restoration: the Regularizing Operator Approach, Optical Engineering, 28, 7, 1989, pp. 761-780.
13. Franklin, J.N., Well-Posed Stochastic Extensions of Ill-Posed Linear Problems, J. Math. Anal. Applications, 31, 1970, pp. 682-716.
14. Mohammad-Djafari, A. and Demoment, G., Maximum-Entropy and Bayesian Methods in Science and Engineering, 2, Kluwer Academic Pub., 1985, p. 341.
15. Anteneodo, C. and Plastino, A.R., Maximum Entropy Approach to Stretched Exponential Probability Distributions, J. Phys. A., 32, 1999, pp. 1089-1097.
16. Kapur, J.N. and Kesavan, H.K., Entropy Optimization Principles with Applications, Academic Press, New York, 1992, p. 389.
17. Tsallis, C., Possible Generalization of Boltzmann-Gibbs Statistics, J. Stat. Phys., 52 (1-2), 1988, pp. 479-487.
18. Curado, E. and Tsallis, C., A Generalized Statistical-Mechanical Connection with Thermodinamics, J. Phys. A, 24 (2), 1991, pp. L69-L72.

19. Bregman, L.M., The Relaxation Method of Finding the Common Point of Convex Sets and its Application to the Solution of Problems in Convex Programming, USSR Computational and Mathematical Physics, 7, 3, 1967, pp. 200-217.
20. Carita Montero, R.F., Roberty, N.C. and Silva Neto, A.J., Natural Base Construction for Absortion Coefficient Estimation in Heterogeneous Participating Media with Divergent Beams, Proc. 3rd International Conference on Inverse Problems in Engineering: Theory and Practice, Port Ludlow, Washington, USA, 1999.
21. Frieden, B.R., Restoring with Maximum Likelihood and Maximum Entropy, J. Opt. Soc. Am., 62, 4, 1972, pp. 511-518.
22. Silva Neto, A.J. and Moura Neto, F.D., Model Choosing – Inverse Problems in Engineering, Published by the Brazilian Society of Applied and Computational Mathematics (SBMAC) as lectures notes of the 22nd Brazilian Congress of Applied and Computational Mathematics, in portuguese, 1999.
23. Kirsch, A., An Introduction to the Mathematical Theory of Inverse Problems, Springer Verlag, New York, 1996.

Figure Captions:

Figure 1. Image restoration algorithm.
Figure 2. AFM true 1μm x 1μm image of an eritroblast in leukemia pathology.
Figure 3. Restored image using a 9 x 9 DGM (σ^2=10), with α=0.03 and γ=0.2.
Figure 4. AFM true 600 nm x 600 nm image of an eritroblast in leukemia pathology.
Figure 5. Restored image using a 9x 9 DGM (σ^2 =10), with α=0.03 and γ=0.2.
Figure 6. Restored image using a 15 x 15 DGM (σ^2=40), with α=0.03 and γ=0.2.

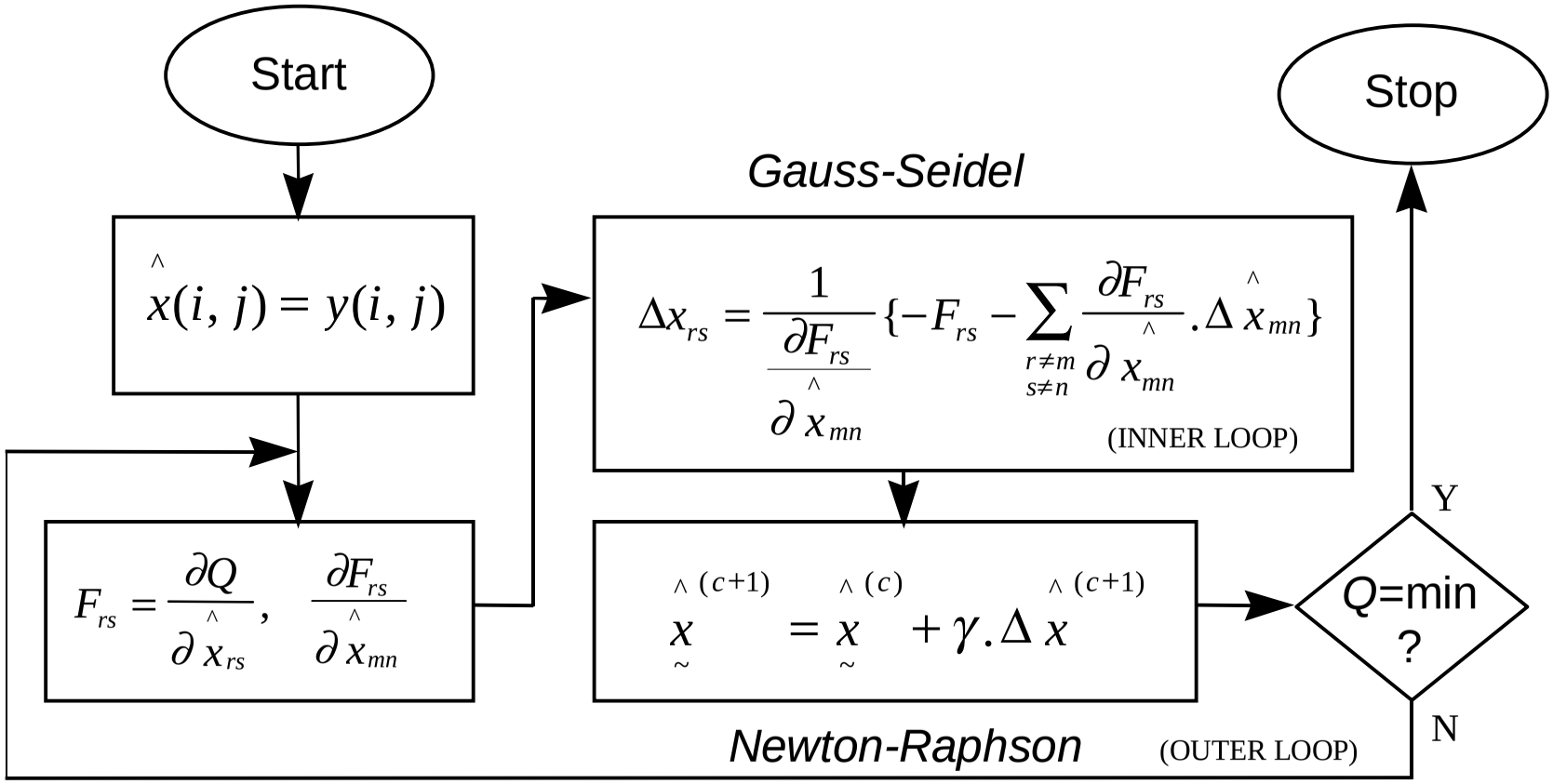
Start
$\hat{x}(i,j) = y(i,j)$
$F_{rs} = \frac{\partial Q}{\partial \hat{x}_{rs}}, \quad \frac{\partial F_{rs}}{\partial \hat{x}_{mn}}$
Gauss-Seidel
$\Delta x_{rs} = \frac{1}{\frac{\partial F_{rs}}{\partial \hat{x}_{mn}}} \{-F_{rs} - \sum_{\substack{r \neq m \\ s \neq n}} \frac{\partial F_{rs}}{\partial \hat{x}_{mn}} . \Delta \hat{x}_{mn}\}$
(INNER LOOP)
$\underset{\sim}{\hat{x}}^{(c+1)} = \underset{\sim}{\hat{x}}^{(c)} + \gamma . \Delta \hat{x}^{(c+1)}$
Newton-Raphson
(OUTER LOOP)
Q=min ?
Y
N
Stop

FIGURE 1

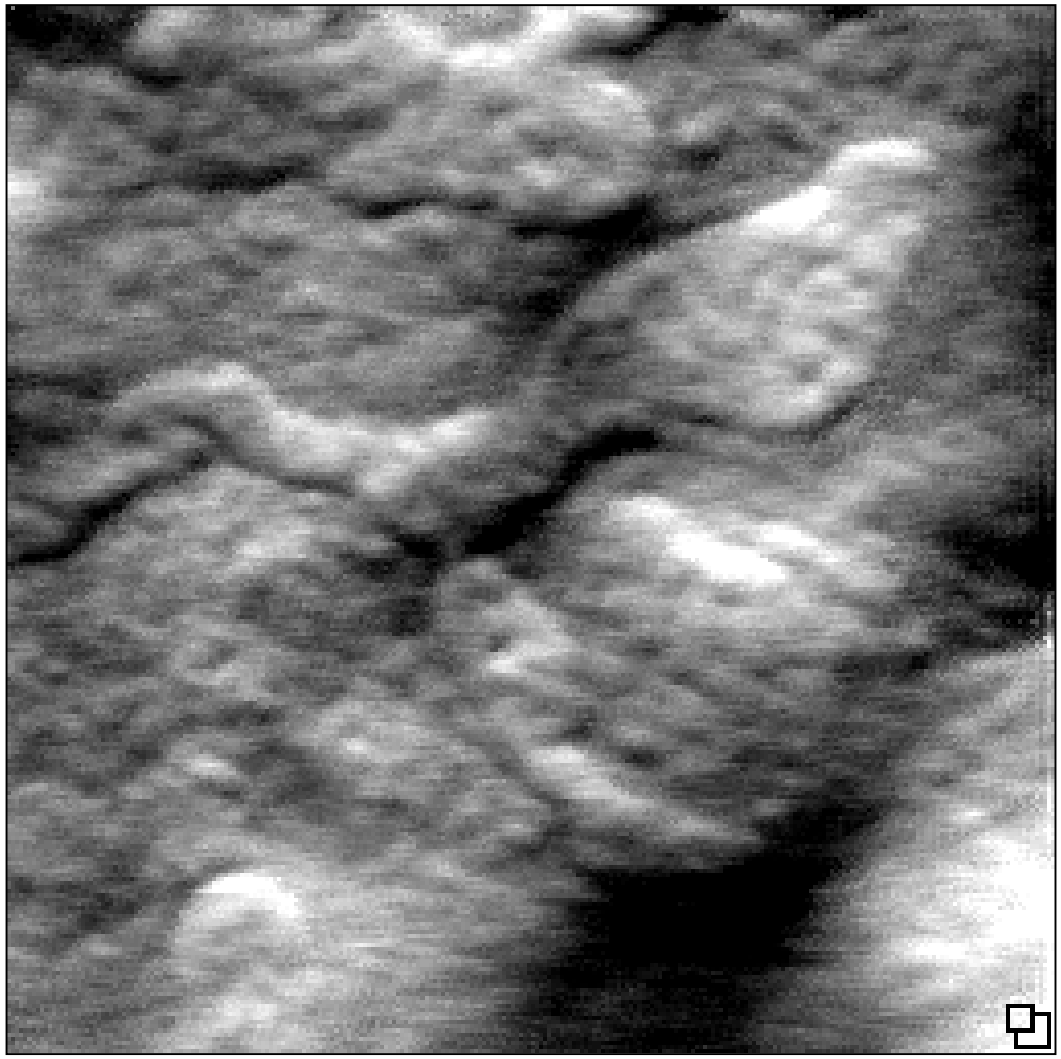

FIGURE 2

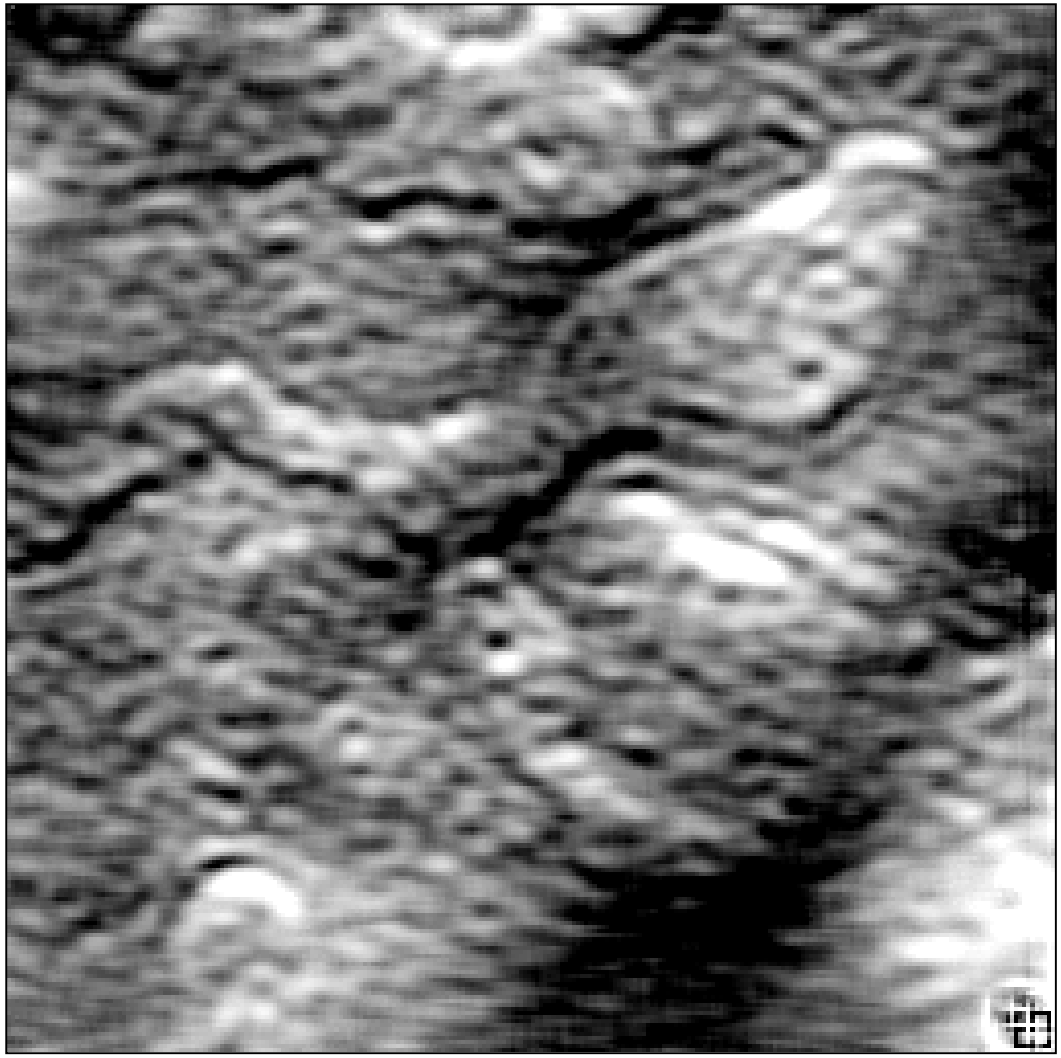

FIGURE 3

FIGURE 4

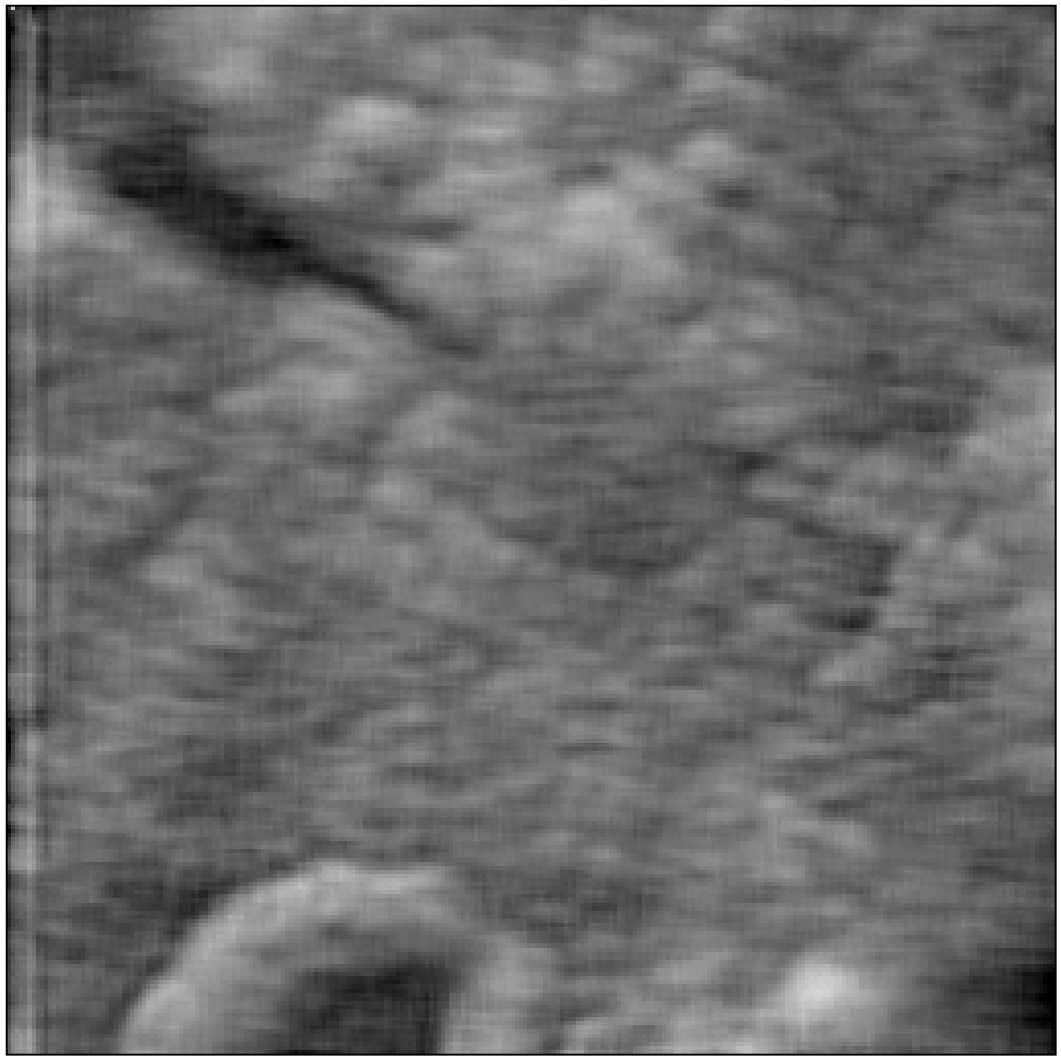

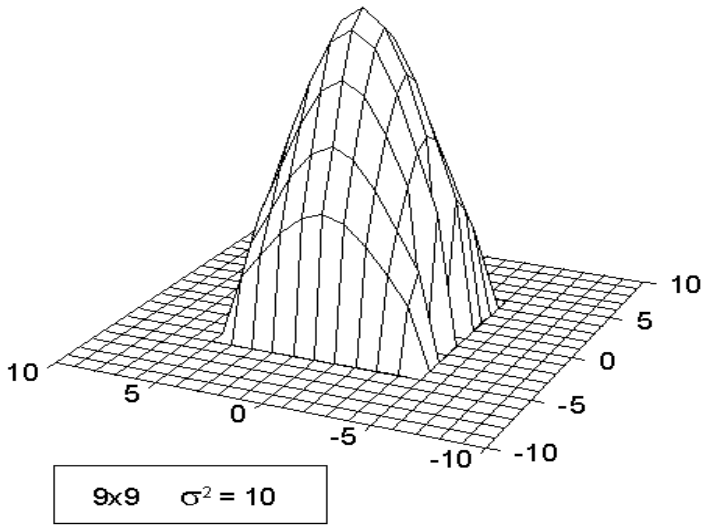

FIGURE 5

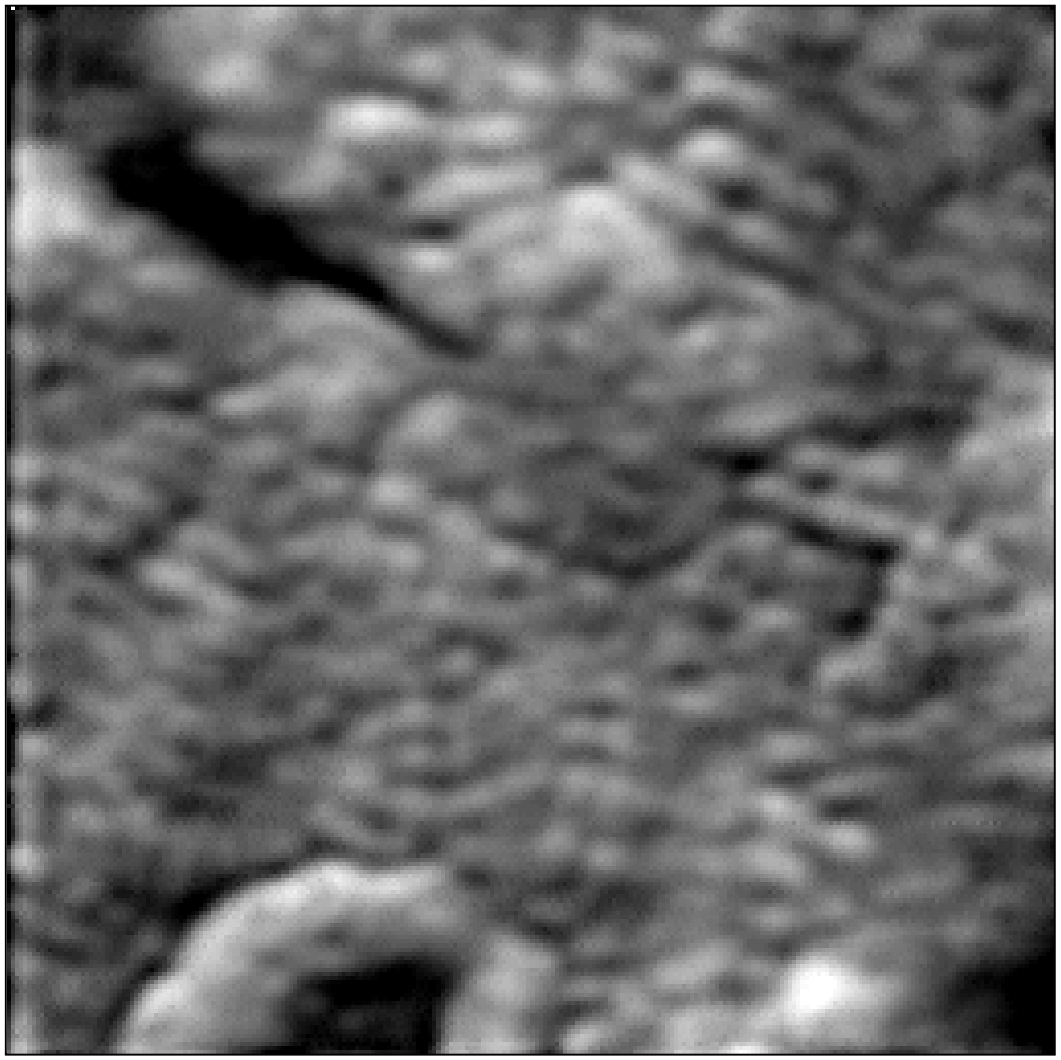

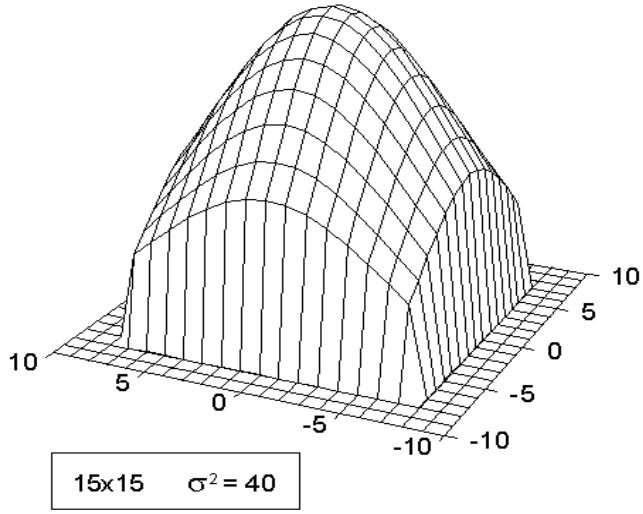

FIGURE 6